Lipoproteins LDL versus HDL as nanocarriers to target either cancer cells or macrophages

Tarik Hadi, Christophe Ramseyer, Thomas Gautier, Pierre-Simon Bellaye, Romain Douhard, Lucile Dondaine, Lil Proukhnitzky, Samir Messaoudi, F. Neiers, Laurent L. Lagrost, et al.

Lipoproteins LDL versus HDL as nanocarriers to target either cancer cells or macrophages

Hadi T [1,2,3], Ramseyer C [2,4], Gautier T [1,2], Bellaye PS [5], Lopez T[1,2], Schmitt A[1,5], Foley S [2,4], Yesylevskyy S [4,6], Minervini T [2,4], Douhard R[1,2], Dondaine L[1,2], Proukhnitzky L[1,2], Messaoudi S[10], Wendremaire M[1,2], Moreau M[8], Neiers F[7], Collin B[2,5], Denat F[8], Lagrost L[1,2]*, Garrido C[1,2,5]*# & Lirussi. F[1,2,9]*#

1: INSERM, U1231, Label LipSTIC, and Ligue Nationale contre le Cancer, Dijon, France

2: Université de Bourgogne-Franche Comté, France

3: NYU Langone Medical Center, department of Vascular Surgery, New York, NY, USA

4: Laboratoire Chrono Environnement UMR CNRS 6249, Université de Bourgogne Franche-Comté, 16 route de Gray, 25030 Besançon Cedex, France.

5: Anti-cancer Center George-François Leclerc, CGFL, Dijon, France

6: Department of Physics of Biological Systems, Institute of Physics of the National Academy of Sciences of Ukraine, Prospect Nauky 46, 03028 Kyiv, Ukraine

7: Centre des Sciences du Goût et de l'Alimentation, INRA, CNRS, Bourgogne Franche-Comté University, France

8: ICMUB, Institut de Chimie Moléculaire de l'Université de Bourgogne, UMR6302, CNRS, Université Bourgogne Franche-Comté, 9 avenue Alain Savary, 21000, Dijon, France

9: University Hospital of Besancon (CHU)

10: BioCIS, Univ. Paris-Sud, CNRS, Univ. Paris-Saclay, Châtenay-Malabry, France

The authors declare no potential conflicts of interest.

[#] **Corresponding Author at:**

Frederic Lirussi

INSERM, U1231

UFR des Sciences de Santé

7, Bd Jeanne d'Arc, BP 87900

21079 DIJON Cedex, FRANCE

Frederic.Lirussi@u-bourgogne.fr

&

Carmen Garrido

INSERM, U1231

Label LipSTIC, and Ligue Nationale contre le Cancer

7, Bd Jeanne d'Arc, BP 87900
21079 DIJON Cedex, FRANCE
cgarrido@u-bourgogne.fr

* Co-supervising of the work

Main text

Abstract

In this work, we have explored natural unmodified low- and high-density lipoproteins (LDL and HDL) as selective delivery vectors in colorectal cancer therapy. We show *in vitro* in cultured cells and *in vivo* (NanoSPECT/CT) in the CT-26 mice colorectal cancer model that LDLs are mainly taken up by cancer cells, while HDLs are preferentially taken up by macrophages. We loaded LDLs with cisplatin and HDLs with the heat shock protein-70 inhibitor AC1LINNC, turning them into a pair of "Trojan horses" delivering drugs selectively to their target cells as demonstrated *in vitro* in human colorectal cancer cells and macrophages, and *in vivo*. Coupling of the drugs to lipoproteins and stability was assessed by mass and raman spectrometry analysis. Cisplatin vectorized in LDLs led to better tumor growth suppression with strongly reduced adverse effects such as a renal or liver toxicity. AC1LINNC vectorized into HDLs induced a strong oxidative burst in macrophages and innate anti-cancer immune response. Cumulative anti-tumor effect was observed for both drug-loaded lipoproteins. Altogether, our data show that lipoproteins from patient's blood can be used as natural nanocarriers allowing cell specific targeting, paving the way toward more efficient, safer and personalized use of chemo-and immunotherapeutic drugs in cancer.

Key words: Lipoproteins, vectorization, selective cell targeting, cisplatin, heat shock protein inhibitor, cancer therapy

Introduction

Among promising immunotherapeutic approaches in cancer are those targeting macrophages. Macrophages are present in substantial amounts in most solid tumors and influence tumor growth or regression through inflammatory and metabolic switch (1, 2). Macrophages, depending on their inflammatory status, can have a phenotype either tolerogenic (pro-tumoral) or cytotoxic (anti-tumoral). Those that infiltrate the tumor are tolerogenic. Switching the polarization of those macrophages so they become cytotoxic is being investigated by many scientists (3). We recently demonstrated that the stress-inducible heat shock protein-70 (HSP70) was abundantly secreted by tumor cells and favored pro-tumor phenotype in macrophages. Accordingly, depletion of HSP70 induced tumor regression via a massive intra-tumor recruitment of cytotoxic macrophages (4).

Concerning cancer chemotherapy, platinum-derived drugs such as cisplatin are major compounds in cancer treatment, particularly in colorectal cancer. However, besides high efficiency, cisplatin cytotoxicity causes cellular damage in healthy tissues, leading to adverse side effects such as renal and liver failure(5), pulmonary fibrosis or increased cardiovascular events (6), dramatically limiting the dose of cisplatin that can be used on patients, thereby limiting its efficacy.

More specific cell targeting, toxicity and solubilization issues have prompted the development of nanovectorization approaches. Hence, cisplatin encapsulation into liposomes is considered a promising strategy to reduce the amount of free cisplatin in the plasma and specifically delivering it to target tissues. While most of these attempts did not show significant toxicity reduction, a few studies successfully passed phase II clinical trials but still need phase III validation (7). Another approach to improve cisplatin efficacy in colon cancer treatment has been recently proposed through the creation of orally-administered squalenoylated nanoparticles loaded with cisplatin (8).

In contrast to these artificial lipid nanovectors, in this work we have explored natural lipoproteins (LDL and HDL) as nanocarriers for colorectal cancer drugs. We studied cisplatin and the potential immunotherapeutic HSP70-targetting drug (AC1LINNC) binding to purified native human

lipoproteins, and the influence of such complexation on their selective transport to colorectal cancer cells or macrophages.

Results

Pharmacodynamics parameters of LDL and HDL

We first determined the pharmacodynamics (PK) parameters of lipoproteins in Balb/c mice to choose the optimal time for tissue distribution assessment. Purified HDLs and LDLs were labelled with DOTA-Bodipy-NCS and injected *i.v.* into mice. Mean concentration time courses are presented in Figure 1A-B. PK parameters were relatively consistent between animals for HDL (Figure 1A, Supplementary table 1). Parameters were more variables between animals for LDL (Figure 1B, Supplementary table 2), due to a rapid decrease in labeled-LDL-concentration during the first minutes following *i.v.* injection. Cmax was rapidly reached after HDL *i.v.* injection and was about 0.09 mg/mL for a dose of 0.615 mg. Mean exposure between the first and the last measurements (*i.e.*, AUClast) was equal to 45.79 mg/mL.min and represented about 80% of the total exposure. Clearance was low, leading to a median terminal half-life of 14h. After 300 minutes, LDL concentrations were not always quantifiable. Mean exposure between the first and the last measurements (*i.e.*, AUClast) was equal to 4.73 mg/mL.min. Clearance was higher than for HDL, with a median terminal half-life of about 10 h.

The goodness-of-fit plots (Figure 1C-D) shows a good correlation between observed and predicted concentrations, assuming that HDL and LDL followed a bicompartmental model. The major variability was linked to the volume of distribution in the central compartment (i.e., blood) (Supplementary table 3). The developed model enabled us to determine the optimal limited sampling strategy for our further experiments.

Tissue distribution and cancer cell specificity of LDL versus HDL in tumor bearing mice

For *in vivo* tissue distribution and cellular uptake of LDL and HDL, lipoproteins were labeled with radiolabeled ^{111}Indium (^{111}In) DOTA-Bodipy-NCS and injected *i.v.* into colorectal CT26 tumor-bearing mice. This was reached 12 days after subcutaneous injection of CT26 cancer cells into the left flank of Balb/c mice. Labeled LDL and HDL *in vivo* distribution was followed by SPECT-CT and fluorescence microscopy. Lipoproteins uptake in the tumor and different organs (liver, spleen, heart, kidneys, bladder and blood) was visualized over 72h in the whole animal (Figure 2A-B). As expected,

the highest levels of both LDLs and HDLs were found in the liver (Figure 2G, Supplemental Data 1A). However, 24h after systemic injections, lipoproteins could be visualized in the tumors, reaching a peak between 48-72 h (Figure 2A&B). HDL and LDL increase in tumors inversely correlated with their decrease in the heart (Figure 2C-F), indicative of lipoprotein decrease in the bloodstream. Of note, low amounts of both HDL and LDL were observed in the bladder throughout the experiment (Supplemental Data 1B), suggesting that both lipoproteins were not rapidly cleared in the urine. It is worth noting that LDL was more difficult to visualize within the tumor most probably because of its much faster clearance (Figure 1B).

We next aimed to determine LDL and HDL subpopulations fates within the tumor. Twelve hours after injection of bodipy-bound HDL and LDL, the tumors were dissociated and submitted to FACS analysis (Figure 3A&B). Interestingly, we observed that LDL-bodipy was preferentially up taken by $CD45^-$ cells, which are predominantly tumor cells, while HDL-bodipy preferentially accumulated in macrophages ($CD45^+/CD11b^+/F4/80^+/Ly6G^-$, Figure 3B). This differential targeting of LDL versus HDL was confirmed *in vitro* using human cultured cells. Indeed, colorectal cancer HCT116 cells preferentially accumulated LDL-bodipy (Figure 3C) while macrophages (from healthy volunteers' buffy coats) mainly up took HDL-bodipy (Figure 3D)

HDL as vectors for potential immunotherapeutic agents such as the HSP70-targetting AC1LINNC.

With the rational that HDLs abundantly accumulated in macrophages, we decided to complex HDL to a molecule that we screened for its ability to target the heat shock protein-70 (HSP70), a chaperone known for its tumorigenic role involving macrophages differentiation/activity(4, 9-11). This molecule, designated as AC1LINNC (Supplemental Data 2A), binds to HSP70 with an IC50 of 0.2µM (Supplemental Data 2C) and inhibits HSP70 chaperone activity (Supplemental Data 2B&D). AC1LINNC is highly hydrophobic and insoluble hampering its use *in vivo,* thereby increasing the interest for its vectorization. We incubated HDL or LDL (1mM cholesterol each) with AC1LINNC (to a final concentration of 100µM) (Supplemental Data 3A). Mass spectrometry analysis revealed a 30% uptake of AC1LINNC by both LDL and HDL allowing to achieve a final concentration of about 30µM

(Figure 4A). To evaluate the stability of AC1LINNC-bound lipoproteins and possible exchange of AC1LINNC between LDL and HDL particles, AC1LINNC-bound LDLs or AC1LINNC-bound HDLs (1mg/ml) were incubated with native HDLs or LDLs (1mg/ml), respectively (Supplemental Data 3B). AC1LINNC was not detected in the newly added native lipoproteins, indicating that the interaction is stable with no exchange with other lipoproteins (Figure 4B). We found that while the AC1LINNC complexed to LDL had no effect, the same amount of the AC1LINNC vectorized in HDL or solubilized in DMSO induced ROS production in macrophages (Figure 4C).

To confirm the *in vivo* potential interest of HDL-bound AC1LINNC, we used the rodent CT-26 colorectal cancer model. CT-26 cells were subcutaneously injected into the left flank of Balb/c mice. Day 0 was considered when tumor size reached about 6 mm^3: at day 10, mice were treated *i.p.* with PBS, HDL-AC1LINNC (1.5mg/kg), LDL-AC1LINNC or native HDL or LDL. Injections were performed every three days until the end of the experiment (D25, for ethical considerations, Figure 4D&E). Consistent with data obtained from cultured macrophages, we observed higher macrophages tumor infiltration with a drastic increase in ROS production, along with a mild induction of apoptosis in cancer cells (Figure 4F-J). That was associated with tumor regression (Figure 4 E), thereby bringing proof of concept of a macrophage guided effect of HDL complexes. Interestingly, we did not observe any effect of LDL-AC1LINNC treatment, or of either native HDL or LDL on tumor growth.

Lipoproteins as nano-vectors for the chemotherapeutic drug cisplatin

We next used cisplatin, an efficient drug whose heavy undesirable effects hamper its use. Lipoproteins were incubated with cisplatin (final concentration of 1mg/ml) for 4 hours at 37°C (Supplemental Data 3A). After dialysis, total cisplatin concentration in lipoproteins was measured by GF-AAS. We observed an integration of 30% and 50% of the initial dose of cisplatin, into LDL and HDL sub-fractions respectively (Figure 5A). As previously described for the AC1LINNC (Supplemental Data 3B) no cisplatin exchange with other lipoproteins was detected (Figure 5B). *In sillico* (Supplemental Data 4A&B and Supplemental table 4) and raman spectroscopy studies (See Supplemental Data 4C) indicated that cisplatin bound cysteine residues of the ApoB-100 protein.

Antitumor *in vivo* effect of cisplatin complexed to LDL

The impact of cisplatin-LDL versus -HDL complexes on *in vitro* tumor cell death was determined by MTT viability test. We observed that LDL-vectorization improved cisplatin-induced cancer cell mortality (Figure 5C), while HDL-vectorization had no effect compared to the control (Supplemental Data 5A). These results were in agreement with our previous data showing that HDLs were not captured by HCT116 tumor cells while LDLs hardly entered macrophages. Consistently, we observed that cisplatin complexed to LDL had no effect on macrophage ROS production (Figure 5D) while HDL-bound cisplatin induced a strong response (Supplemental Data 5B).

This effect of the LDL-cisplatin complexes in tumor cells was further observed *in vivo* in CT-26 tumor-bearing mice (Figure 5E-K). Mice were treated *i.p.* ever 3 days with PBS, native HDL or LDL, cisplatin (Cis-Pt, 1.5mg/kg) or cisplatin (1.5mg/kg) complexed to LDL (LDL-Cis) or HDL (HDL-Cis), (Figure 5E). LDL-Cis treatment was associated with a stronger tumor regression than cisplatin alone (Figure 5F), while no significant effects of HDL-Cis or native lipoproteins were observed on tumor growth (Supplemental Data 5C). Consistently, we observed that LDL vectorization of cisplatin was associated with a higher tumor cell death (caspace-3, Figure 5G&I) and a higher proportion of macrophages infiltrating the tumor (F4/80, Figure 5G&J), compared both to control and non-vectorized cisplatin groups. Interestingly, cleaved-caspase-3 staining did not co-localize with F4/80, suggesting a selective pro-apoptotic effect on tumor cells. Additionally, this pro-apoptotic effect was associated with increased ROS production as assessed by DHE/DAPI staining (Figure 5H&K). To summarize, LDL vectorization improves the efficiency of cisplatin, by increasing tumor cell death and, most probably indirectly, favoring cytotoxic macrophage infiltration.

Vectorization of cisplatin by LDL strongly diminishes cisplatin adverse side effects

To investigate the impact of lipoprotein vectorization on cisplatin nephrotoxicity, mice were treated with cisplatin using a standardized kidney injury protocol. Tumor-bearing mice were injected with a single dose of 30 mg/kg cisplatin and euthanized at day 3. Toxicity was assessed by evaluating weight loss and renal dysfunction (Figure 6A). Mice treated with Cis-Pt experienced a 19% weight loss

only 3 days following injection. In contrast, mice treated with LDL-bound cisplatin did not experience any weight loss (Figure 6B), while, interestingly, no decrease in cisplatin anti-cancer drug efficiency was observed (Figure 6C).

Following cisplatin treatment, mice displayed distortion of the overall renal morphology, dilation of renal tubules, and appearance of protein cast, most of which were significantly attenuated in the cisplatin lipoprotein-vectorized group (Figure 6D&E). In addition to these observations, apoptosis assessed by caspase-3 cleavage was dramatically decreased in the kidney of mice treated with cisplatin complexed to LDL (Figure 6F&G), while the induction of apoptosis in tumor cells was comparable in both groups (Figure 6F&H). Furthermore, since the liver is involved in lipoprotein turnover, we aimed to assess if cisplatin complexed to LDL would induce hepatic toxicity. Interestingly, we found that LDL-bound cisplatin did not induce hepatic toxicity, as shown by comparing apoptosis (cleaved caspase-3) in the liver of animals treated with cisplatin versus LDL-cisplatin (Supplemental Data 1B&C). Altogether, cisplatin complexed to LDL, while preserving cisplatin anti-tumor effect, displays a reduced side effect toxicity.

Combinational effect of AC1LINNC-HDL and cisplatin-LDL complexes

Finally, we tested the impact of the association of cisplatin-LDL complexes together with AC1LINNC-HDL complexes. Tumor-bearing mice were treated with LDL-Cisplatin, HDL-AC1LINNC or the combination of both. While we did not observed a stronger decrease in tumor growth when using the combinational therapy (Figure 7A&B), immunofluorescent staining revealed i) a strong induction of cancer cell apoptosis (Figure 7C&E), comparable to that observed in the animals treated with LDL-Cisplatin alone ii) a strong burst in macrophage infiltration (Figure 7C&F) comparable to HDL-AC1LINNC alone. This suggests that this combined strategy aiming to simultaneously target cancer cells with one drug (cisplatin-LDL) and tumor-infiltrating macrophages with the other (AC1LINNC-HDL) allows a complementary additive effect that could prove more efficient during prolonged treatment.

Discussion

In the field of cancer treatment, liposomal encapsulation of lipophilic drugs such as doxorubicin (Doxil, AmBisome) or vincristine (Marquibo) led to improved efficacy and safety. These new formulations were approved by the US Food and Drug Administration (12, 13). However, the use of liposomal carriers for hydrophilic cisplatin has not achieved these goals so far. Among the few liposomal formulations of cisplatin that reached clinical trials, encapsulation of cisplatin in SPI-77® liposomes did not produce significant clinical efficacy in phase II studies despite its safer toxicity profile (14), due to inefficient release of the drug from the carrier (15). Although Lipoplatin® (active encapsulation of cisplatin into PEGylated liposomes) showed enhanced antitumor efficacy compared to free cisplatin in some patients along with reduced renal toxicity, phase II and III studies demonstrated inconsistent effects on survival rates (16). Finally, LiPlaCis®, a phospholipase A2-sensitive liposomal cisplatin carrier have shown a poor safety profile, leading to the discontinuation of phase I studies (17).

In the present study, we considered native human LDL and HDL as carriers for several reasons: 1) lipoproteins are endogenous, physiological and stable molecular complexes that can carry a wide variety of molecules in the bloodstream; 2) they bear specific apolipoproteins that allow targeting to specific receptors; 3) certain chemotherapeutic drugs such as cisplatin display affinity for plasma proteins and therefore are likely to bind to apolipoproteins (18). This latter hypothesis was supported in the present work by *in silico* studies showing that hydrophobic cisplatin interacts with the protein moiety, and not the lipid moiety of lipoproteins. Further, we demonstrate *in vitro* that cisplatin association to LDL and HDL is highly efficient and stable in aqueous solution, with no subsequent release of bound cisplatin into the buffer or towards other non-loaded lipoproteins. These results, together with our *in vivo* kinetics experiments suggest that cisplatin binding to lipoproteins can significantly prolong its half-life in the blood (only 0.24 hours for free cisplatin (19)). This may allow the molecule to reach its target tissue instead of being quickly cleared in an unspecific manner. Accordingly, we were able to show that substantial amounts of labeled lipoproteins could be found within CT-26 tumors after their systemic administration in mice.

Interestingly, LDL and HDL targeted different cells within the tumor. While labeled HDL preferentially accumulated in tumor macrophages, LDL were mainly found within CT-26 cancer cells. A possible explanation is that LDL receptor (LDL-R) expression is abnormally elevated in cancer cells (20, 21). In contrast, HDL, which uptake cholesterol excess from peripheral cells back to the liver, have been shown to interact with immune cells *via* specific membrane transporters and scavenger receptors, particularly present in macrophages. The specific tropism of the LDL for tumor cells may explain the practically lack of cisplatin's side effects such as renal and hepatic toxicity, when conjugated to LDL.

Since HDL particles are abundantly taken up by macrophages, we believe that loading of HDL with immunotherapeutic compounds may be more promising than with chemotherapeutic drugs. Thus, HDL might have a strong therapeutic interest to vectorise molecules that influence macrophages polarization toward an anti-tumor phenotype, and proof of the concept is shown in this work with an HSP70 inhibitor affecting macrophages differentiation/activation (9, 10). Overall, we conclude that the usage of HDL might allow in the future a more targeted/safer administration into the patient of immunotherapeutic agents alone or in combination with LDL-vectorized chemotherapeutic agents, such as cisplatin.

Methods

Cell culture and mice

HCT116 cells (CCL-247^{TM}) were from the American Type Culture Collection (ATCC). Human macrophages were isolated from healthy donor Buffy Coats (EFS Besançon, France) and differentiated as described(22). 6–8-week-old female Balb/c mice were from Charles River. Mouse colon carcinoma cells CT26 (CRL-2638^{TM} ATCC) were injected subcutaneously in the left flank. Time 0 was considered when tumor size reached 6 mm^3. Mice were treated with cisplatin (1.5 mg/kg), or LDL-Cis (100µM cholesterol, 1.5mg/kg cisplatin). For toxicity experiments, mice were injected *i.p.* at day 10 with PBS, Cisplatin (20 mg/kg), or LDL-Cis (100µM cholesterol, 20mg/kg cisplatin). Tumors were measured every three days. Experiments were approved by the ethical comity of the Université de Bourgogne (protocol N3613).

Lipoprotein purification

LDL and HDL were purified from plasma (EFS Besançon, France) as described(23). For bio-distribution experiments, lipoproteins were labelled with DOTA-Bodipy(24), a fluorescent probe (excitation/emission spectra (522/529 nm maxima) combined to a radioactive trap. Briefly, LDL or HDL (2mg of protein) were incubated 4 hours at 37°C in bicarbonate buffer containing 565µg DOTA-Bodipy(25). Bicarbonate buffer and unbound label were removed and lipoproteins recovered in sterile PBS by filtration in centrifugal concentration tubes (30kDa cutoff Centricon, Merck-Millipore).

Cisplatin and AC1LINNC incorporation in lipoproteins:

Cisplatin (Sigma Aldrich, 479306-1G) was dissolved in 0.9%NaCl to a 10mg/ml concentration. AC1LINNC was diluted DMSO to a 100µM concentration. Cisplatin or AC1LINNC solutions were diluted 10 times in 1mM LDL or HDL fractions and incubated 4 hours at 37°C. Unbound Cisplatin, AC1LINNC and DMSO were removed by successive dialyses using Spectrum™ Spectra/Por™ 1 RC Dialysis Membrane Tubing (6000-8000Da cutoff, Fisher Scientific, 08-670C). For LDL/HDL Cisplatin exchange assays, Cisplatin-bound LDL or Cisplatin-bound HDL (1µM) were incubated 24 hours at 37°C with native HDL or LDL (1µM). Cisplatin incorporation in LDL and HDL was then assessed by GF-

AAS (graphite furnace coupled to atomic absorption spectrophotometry) and AC1LINNC incorporation by mass spectrometry.

Bio-distribution and pharmacokinetics imaging

Tumor bearing Balb/c mice (~300mm^3) received 5µg ^{111}In-DOTAGA-HDL or ^{111}In-DOTAGA-LDL (8−10MBq) *i.v.*. SPECT/CT dual imaging was performed 1h, 24h and 72h after injections using a NanoSPECT/CT small animal imaging tomographic γ-camera (Bioscan Inc., Washington, DC). Mice were anaesthetized with isoflurane (1.5−3% in air) and positioned in a cradle. CT (55 kVp, 34 mAs) and helical SPECT acquisitions were performed in immediate sequence. Both indium-111 photopeaks (171 and 245keV) were used with 10% wide energy windows. Radioactivity was measured (from blood, tumor, and organs) with a scintillation γ-counter. Data were then converted to percentage of injected dose per gram of tissue (%ID/g). SPECT/CT fusion image was obtained using the InVivoScope software (Bioscan Inc.). Radioactivity contents from image analysis were expressed in Bq/g, converted to percentage of injected dose, and compared to those determined by *ex vivo* counting.

Statistical analysis

Differences among two groups were determined using two-tailed unpaired Fisher's t-test, and ANOVA followed by Bonferroni's multiple comparison test for more than two groups, using SigmaStat version 3 (GraphPad Software). Differences were considered significant when $p < 0.05$.

Funding

The work was supported by a French Government grant managed by the French National Research Agency under the program “Investissements d’Avenir” with reference ANR- 11-LABX-0021 (LabEX LipSTIC). We also thank the Conseil Regional de Bourgogne-Franche Comté, the European Union program FEDER, and the "Ligue National contre le Cancer" for their financial support.

Acknowledgments

We thank the Platforms Cellimap for their technical support. S.Y, S.F and C.R. were supported by the European Union’s Horizon 2020 research and innovation programme under the Marie Skłodowska-Curie grant agreement No. 690853. The computational studies work was performed using HPC resources from GENCI- [TGCC/CINES/IDRIS] (Grant 2015-[c2016077586]) and Mésocentre de calcul de Franche-Comté.

Author contribution

TH performed in vitro and in vivo experiments, participated in manuscript redaction. CR, SY, TM performed in silico calculations, FS raman experiments and they all participated in manuscript redaction. TG provided lipoproteins. PSB analyzed radiolabeled images. LT performed in vitro experiments. AS performed pharmacokinetics analyses. RD performed radiolabeled lipoprotein injections, LD participated to in vivo experiments. LP provided lipoproteins. SM provided molecule B, MW and FN dosed the Cisplatin and provided discussion. MM and FD provided bodipy , BC performed radiolabeled mice imaging. LL, CG and FL designed the study, supervised the work and wrote the manuscript.

Figures

Fig. 1.

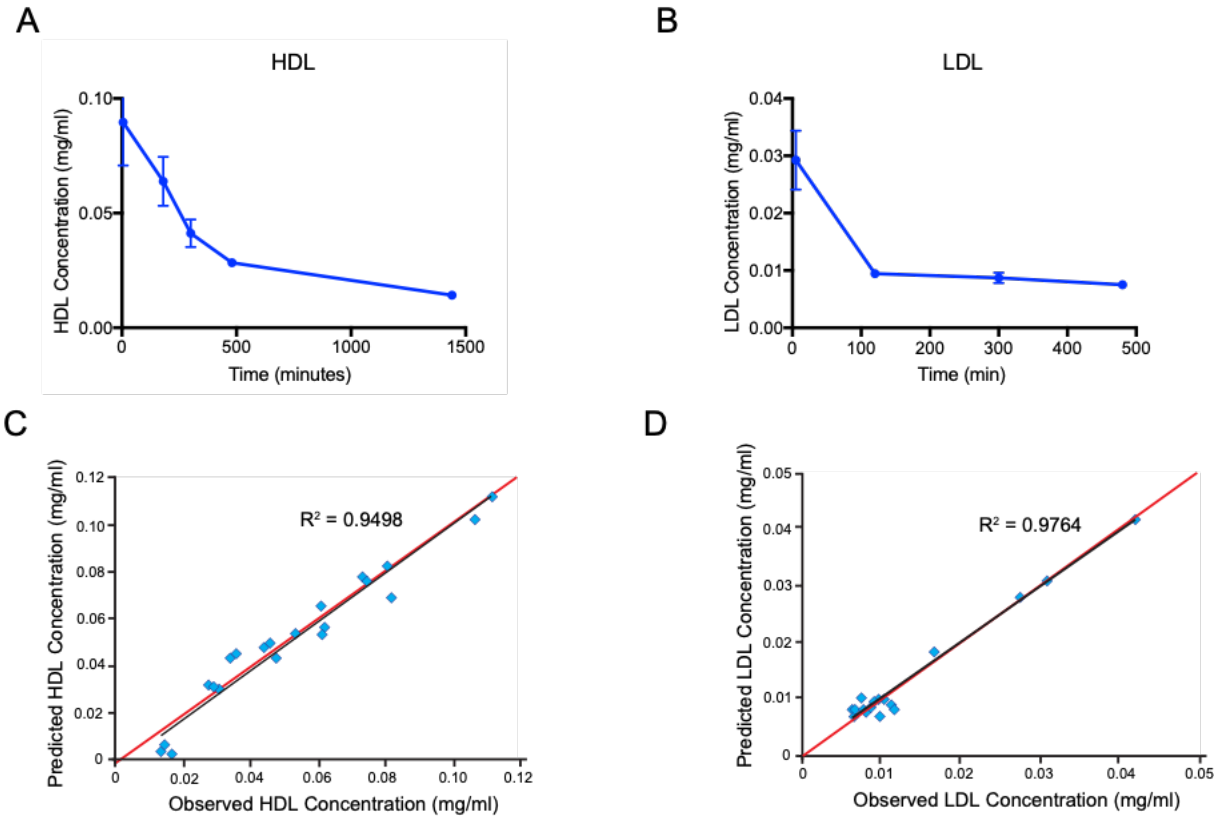

Figure 1: Pharmacokinetics parameters of LDL and HDL in mice. A, B: Balb-c mice were injected *i.v.* with LDL-Bodipy **(A)** or HDL-Bodipy **(B)**, 100µl lipoprotein (1mM cholesterol), 5 mice per group. 100µl of blood sample was dragged at the indicated times. Lipoproteins were extracted by ultracentrifugation, and Bodipy-bound HDL/LDL concentration was assessed by fluorimetry. Values are represented as mean +/- SEM. Mean PK parameters for each condition were compared in order to sort out any differences. **C, D:** In addition to NCA, a population PK approach was used. This approach allows, with a limited number of samples per animal, to determine typical and individual compartmental PK parameters (ka, Cl/F, distribution volume of central compartment, inter-compartmental clearances and distribution volume of peripheral compartments) and the inter-individual variabilities associated to those PK parameters. Data is presented as correlation between the predicted and observed concentrations of HDL **(C)** and LDL **(D)** using this approach.

Fig. 2.

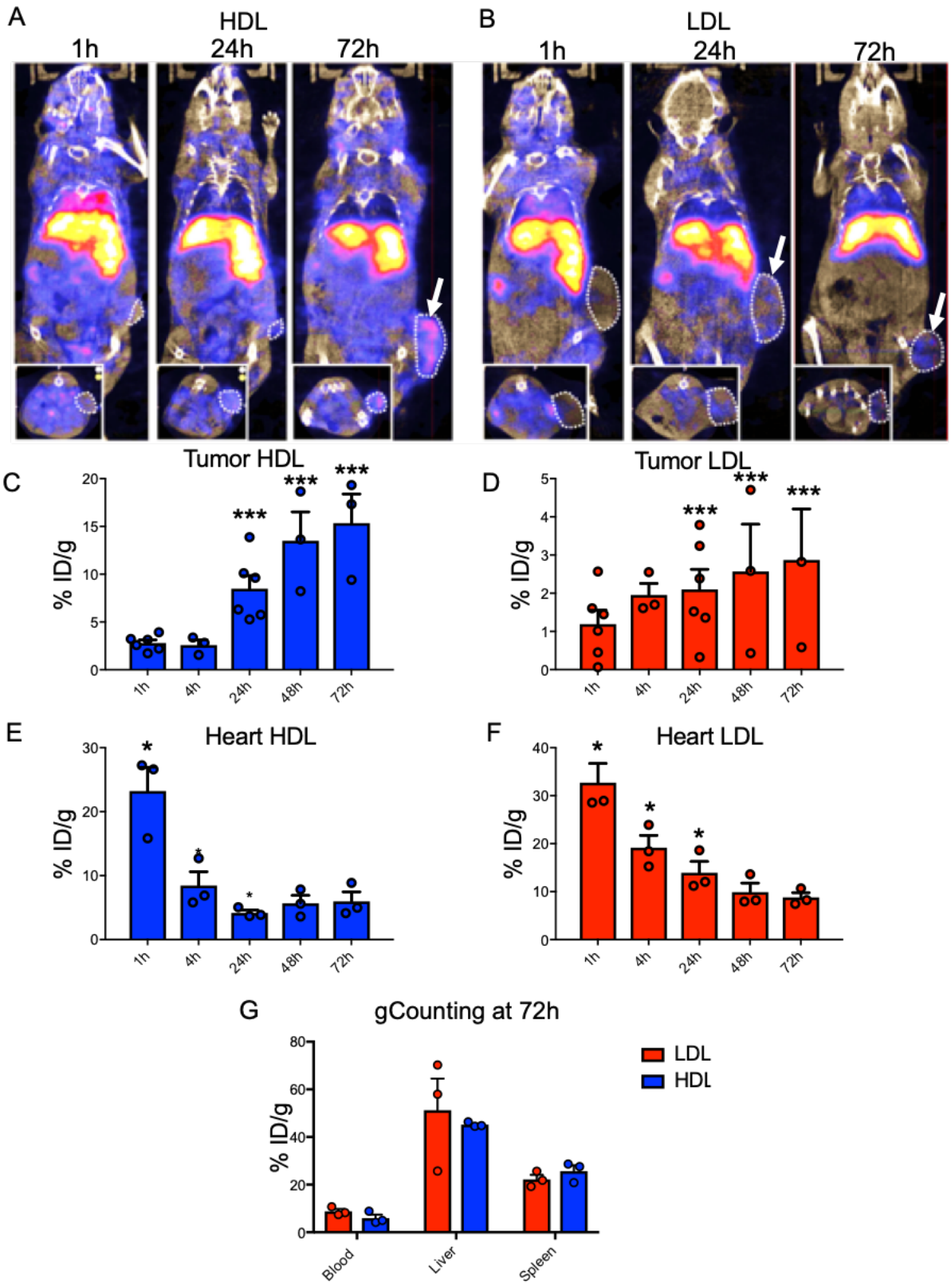

Figure 2. **LDL- and HDL-Bodipy biodistribution in tumor bearing mice. A, B:** Female Balb/c mice (n=3) were grafted by subcutaneous injection of 1.10^6 CT26 colorectal tumor cells. When tumor reached

approximately 300 mm^3, tumor bearing-mice were given 5 µg ^{111}In-DOTAGA-HDL **(A)** or ^{111}In-DOTAGA-LDL (8−10MBq) **(B)** by intravenous injection. SPECT/CT dual imaging was performed 1h, 24h and 72h after the injection of the radiolabeled conjugate using a NanoSPECT/CT small animal imaging tomographic γ-camera. CT (55 kVp, 34 mAs) and helical SPECT acquisitions were performed in immediate sequence. Radioactivity was measured with a scintillation γ-counter from tumor and heart Data were then converted to percentage of injected dose per gram of tissue (%ID/g). SPECT/CT fusion image was obtained using the InVivoScope software. **C, D, E, F & G:** Radioactivity in tumors **(C, E,** n=6**)**, heart **(D, F,** n=3**)**, blood, liver and spleen **(G,** n=3**)** was measured was measured with a scintillation γ-counter. Data is presented as mean value +/- SEM. *$p<0.05$, ***$p<0.001$. *P* values were calculated using one-way ANOVA.

Fig. 3.

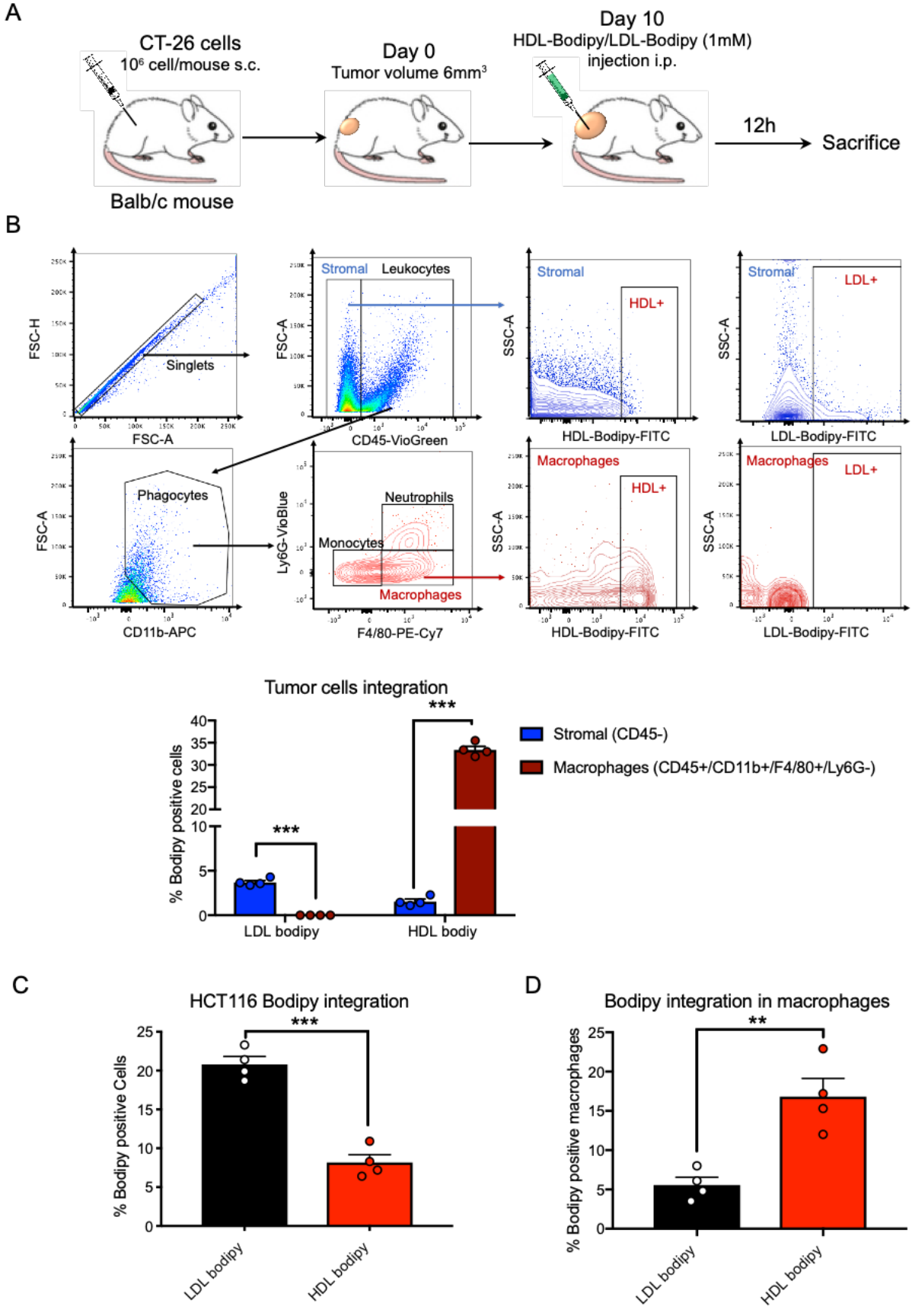
A
CT-26 cells
10⁶ cell/mouse s.c.
Balb/c mouse
Day 0
Tumor volume 6mm³
Day 10
HDL-Bodipy/LDL-Bodipy (1mM)
injection i.p.
12h
Sacrifice
B
FSC-H
FSC-A
Singlets
Stromal
Leukocytes
CD45-VioGreen
SSC-A
HDL-Bodipy-FITC
HDL+
LDL+
LDL-Bodipy-FITC
Phagocytes
CD11b-APC
Ly6G-VioBlue
F4/80-PE-Cy7
Neutrophils
Monocytes
Macrophages
Tumor cells integration
% Bodipy positive cells
Stromal (CD45-)
Macrophages (CD45+/CD11b+/F4/80+/Ly6G-)
LDL bodipy
HDL bodiy
C
HCT116 Bodipy integration
% Bodipy positive Cells
LDL bodipy
HDL bodipy
D
Bodipy integration in macrophages
% Bodipy positive macrophages
LDL bodipy
HDL bodipy

Figure 3: **LDL-bodipy accumulates in cancer cells while HLD-bodipy preferentially target macrophages. A:** Tumor cells and macrophages were isolated by FACS from dissociated CT-26 tumors of mice that have received 24 hours before LDL- or HLD-bodipy (100µM Cholesterol). **B:** Representative gating strategy by flow cytometry for macrophages ($CD45^+/CD11b^+/F4/80^+/Ly6G^-$) and stromal cells ($CD45^-$). Percentages of Bodipy-positive cancer cells (F4/80 negative, blue bars) and macrophages (F4/80 positive, red bars) are represented as mean value +/- SEM. n=4, ***p<0.001. **C, D:** Human coloraectal HCT116 cancer cells **(C)** and human primary macrophages **(D)** were treated for 6 hours with LDL-Bodipy or HDL-Bodipy (100µM Cholesterol). Percentages of Bodipy-positive cells are represented as mean values. n=4, **p<0.01, ***p<0.001. *P* values were calculated using two-tailed unpaired t-tests.

Fig. 4.

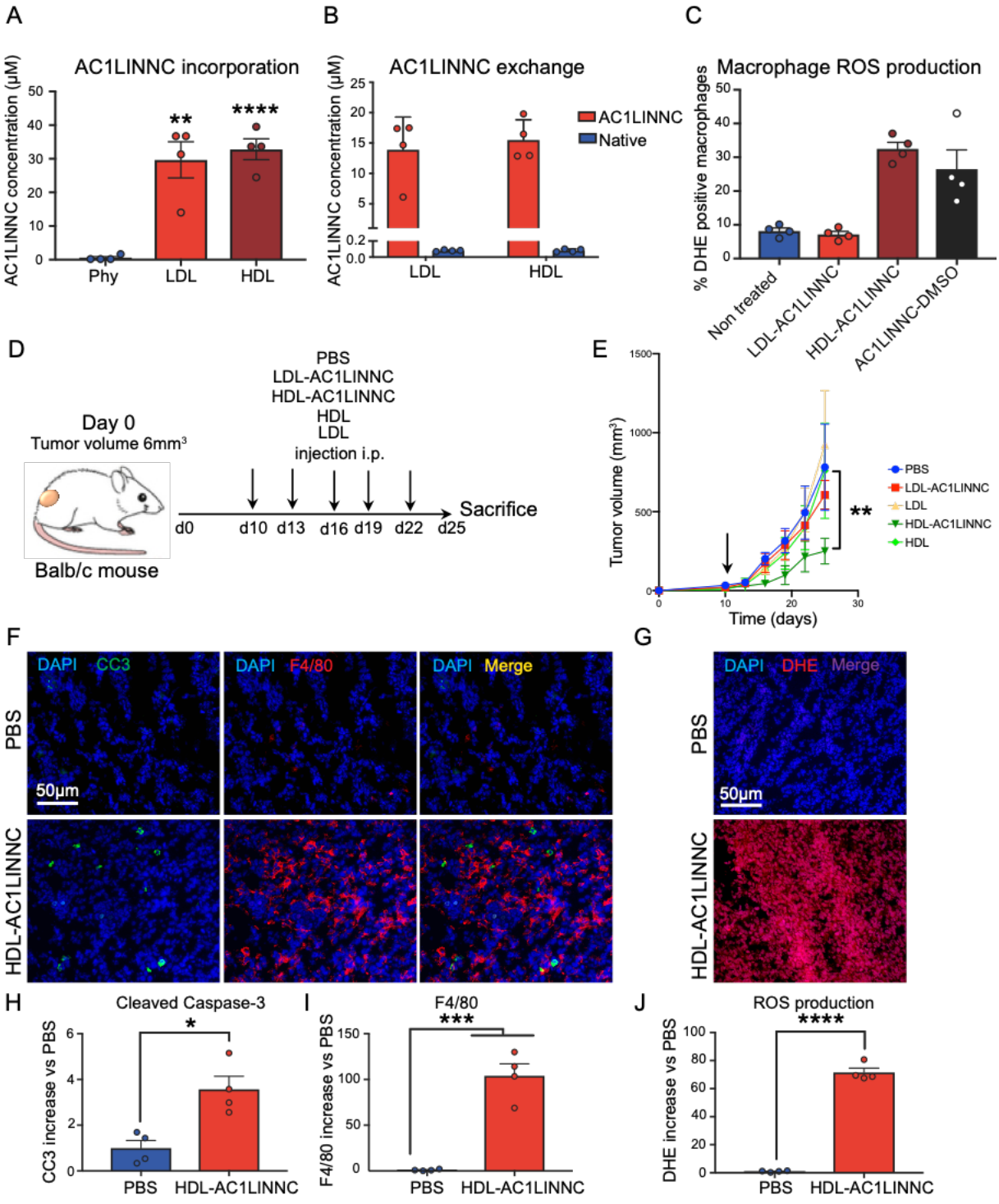

Figure 4: HSP70 inhibitor vectorization in HDL prevents tumor growth by targeting macrophages. A: LDL and HDL were purified by density gradient ultracentrifugation. Total cholesterol in lipoproteins was adjusted to 1mM**.** Lipoproteins were then incubated with AC1LINNC (100µM) for

3 hours at 37°C, then submitted to dialysis. Total AC1LINNC concentration in lipoproteins was then measured by Mass spectrometry. **B:** For AC1LINNC exchanges, after integration, AC1LINNC-bound LDL or AC1LINNC-bound HDL (0,5µM) were incubated for 24 hours at 37°C with native HDL or LDL (0,5µM), respectively. LDL and HDL were purified by density gradient ultracentrifugation, and total cisplatin concentration in lipoproteins was then measured. Data are represented as mean value +/- SEM. n=4, **p<0.01, ***p<0.001. **C:** For macrophages activation, human M2 macrophages were treated for 2 hours with AC1LINNC (10µM in DMSO) or vectorized in LDL or HDL (10µM final AC1LINNC concentration). Percentage of ROS positive macrophages are represented as mean value +/- SEM. n=4, **: p<0.01, NS = Not Significant. **D:** Balb-c mice were injected with CT-26 colorectal cancer cells (10^6 cells/mice, *s.c.*). At the indicated times mice were treated either with HDL-PBS (100µM cholesterol), LDL-AC1LINNC or HDL-AC1LINNC (100µM cholesterol, 10µM AC1LINNC, 100µl/mouse) or native LDL/HDL. n=4. **E:** Tumor volume was measured every 3 days, and represented as mean value +/- SEM, ***: p<0.001, arrow indicates first injection. **F:** Apoptosis and macrophage infiltration were t-determined in histological slides labeled with a cleaved caspase-3 antibody (Green) and a F4/80 antibody (Red), and with DAPI. Pictures were chosen in random fields and are representative of five pictures taken for each condition. n=4, scale bar = 50µm. **G:** ROS production in tumors was measured in histological slides by DAPI/DHE staining. Images, taken in random chosen fields, are representative of five pictures taken for each condition. n=4, scale bar = 50µm. **H, I & J:** Quantifications of the immuno-fluorescence intensity of Cleaved Caspase-3 **(H)**, F4/80 **(I)** and DHE **(J)**. Data are represented as mean increase vs. PBS +/- SEM. n=4, *: p<0.05, ***: p<0.001, ****: p<0.0001. *P* values were calculated using one-way ANOVA **(A, E)** or two-tailed unpaired t-tests **(H, I, J)**.

Fig. 5.

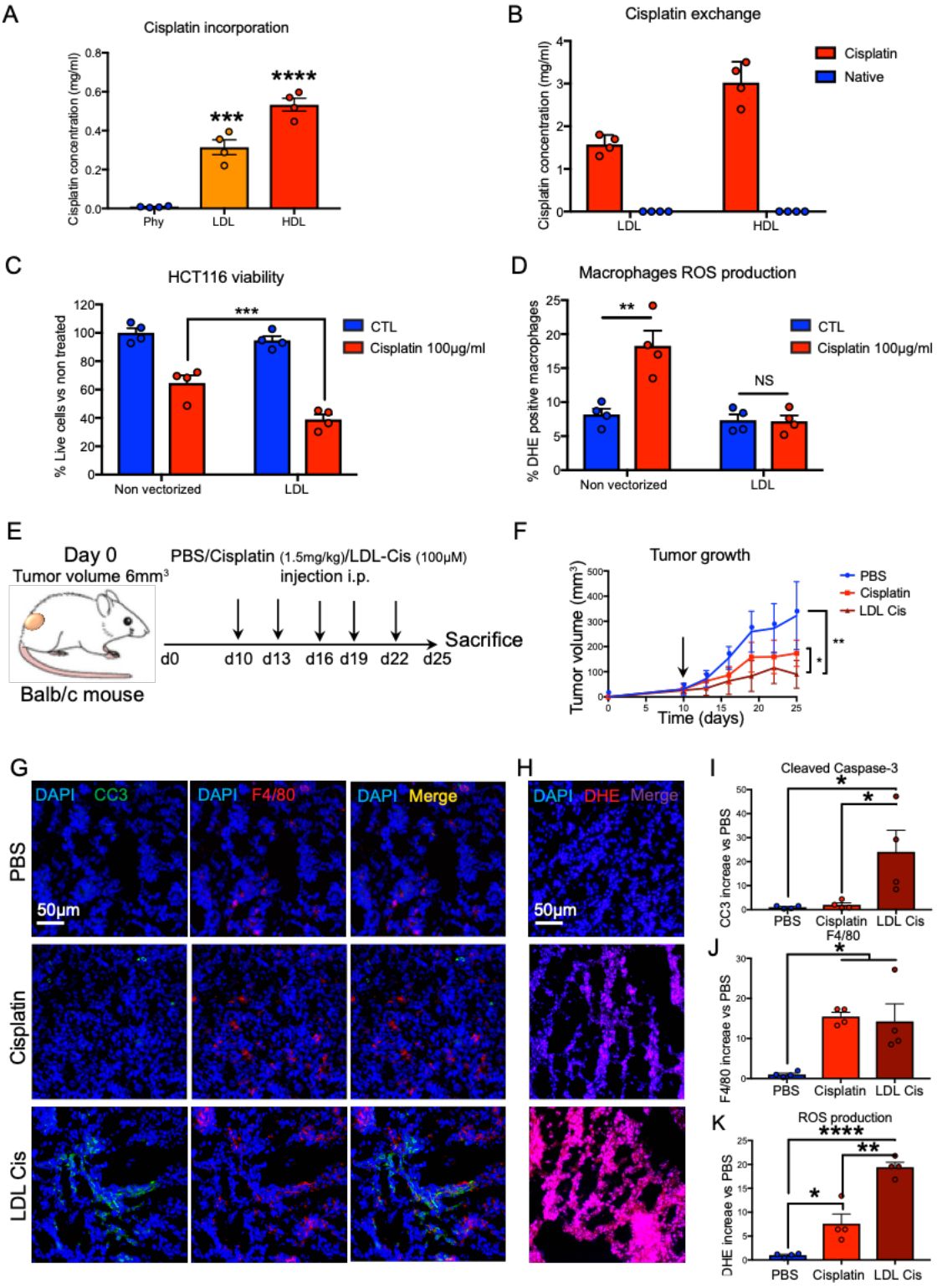

Figure 5: In vivo effects of cisplatin vectorization in LDL. A: LDL and HDL were purified by density gradient ultracentrifugation. Total cholesterol in lipoproteins was adjusted to 1mM**.** Lipoproteins were then incubated with cisplatin (10mg/ml) for 3 hours at 37°C, then submitted to dialysis. Total cisplatin concentration in lipoproteins was then measured by GF-AAS. **B:** For cisplatin exchanges, after

integration, cisplatin-bound LDL or cisplatin-bound HDL (0,5µM) were incubated for 24 hours at 37°C with native HDL or LDL (0,5µM), respectively. LDL and HDL were purified by density gradient ultracentrifugation, and total cisplatin concentration in lipoproteins was then measured. Data are represented as mean value +/- SEM. n=4, ***p<0.001, ***p<0.0001. **C:** For the anti-tumor effect, HCT116 cells were treated for 48 hours with cisplatin alone or vectorized in LDL (25µM final cisplatin concentration). Cell number is represented as mean percentage value vs. non-treated +/- SEM. n=4, ***: p<0.001 vs. non-treated. #: p<0.05 vs. cisplatin alone**. D:** For macrophages activation, human M2 macrophages were treated for 2 hours with cisplatin alone or vectorized in LDL (25µM final cisplatin concentration). Percentages of ROS positive macrophages are represented as mean values +/- SEM. n=4, **: p<0.01, NS = Not Significant. **E:** Balb-c mice were injected with CT-26 colorectal cancer cells (10^6 cells/mice, *s.c.*). At the indicated times mice were treated either with LDL-PBS (100µM cholesterol), cisplatin (1.5 mg/kg), or LDL-Cisplatin (100µM cholesterol, 1.5mg/kg cisplatin). 5 mice/group (n=3). **F:** Tumor volume was measured every 3 days, and represented as mean value +/- SEM, *: p<0.05, **: p<0.01, arrow indicates first injection. **G:** Apoptosis and macrophage infiltration were determined in histological slides labeled with a cleaved caspase-3 antibody (Green) and a F4/80 antibody (Red), and with DAPI. Images were chosen in random fields and are representative of five images taken for each condition. n=5, scale bar = 50µm. **H:** ROS production in tumors was measured in histological slides by DAPI/DHE staining. Images, taken in random fields, are representative of five different ones taken for each condition. n=5, scale bar = 50µm. **I, J & K:** Quantifications of the immune-fluorescence intensity of Cleaved Caspase-3 **(I)**, F4/80 **(J)** and DHE **(K)**. Data are represented as mean increase vs. PBS +/- SEM. n=4, *: p<0.05, ****: p<0.0001. *P* values were calculated using one-way ANOVA **(A, F, I, J, K)** or two-tailed unpaired t-tests **(C, D)**.

Fig. 6.

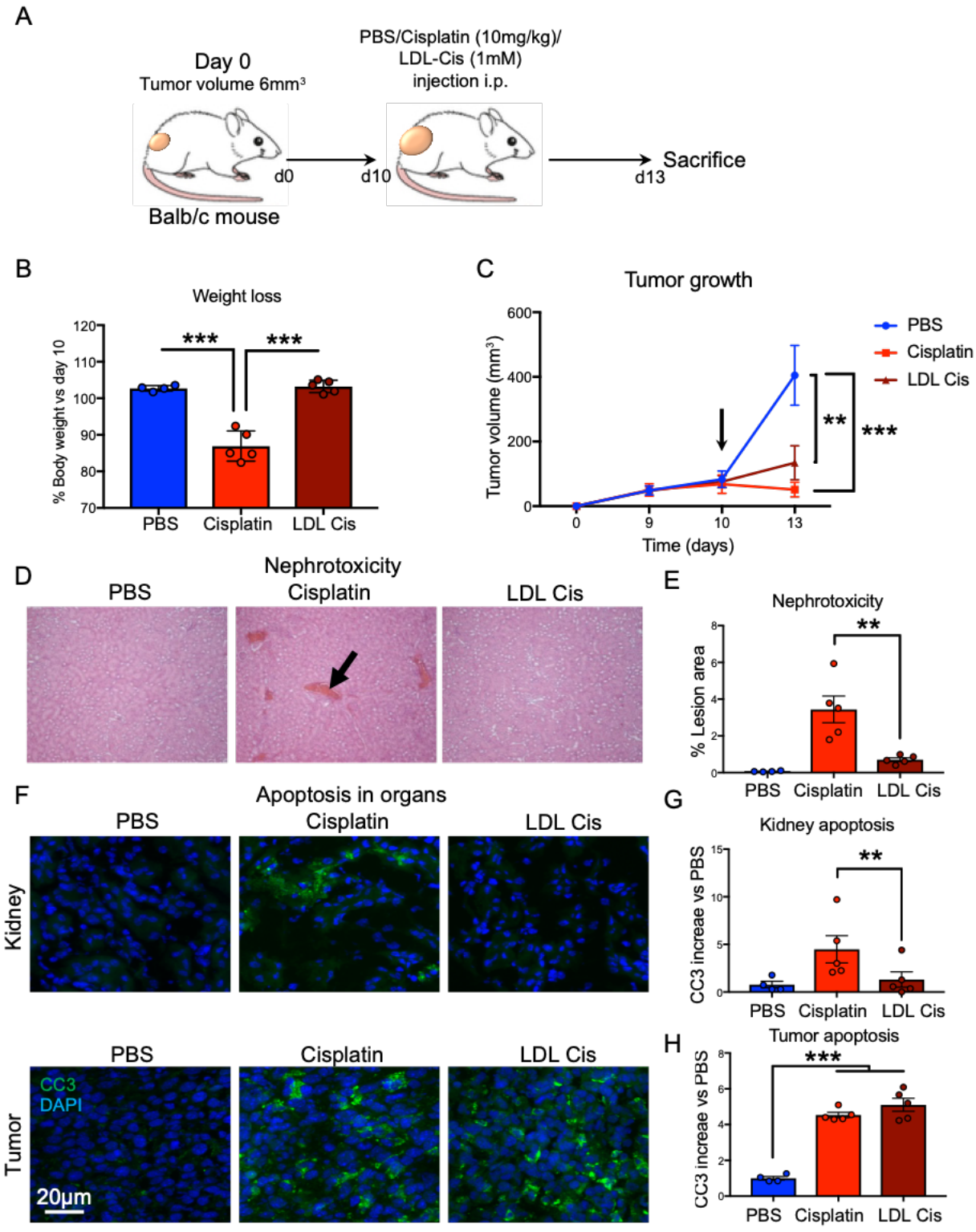

Figure 6: LDL vectorization of cisplatin diminish cisplatin adverse effects. A: Balb-c mice were injected with CT-26 colorectal cancer cells (10^6 cells/mice, *s.c.*). When tumors reached approximately 300 mm^3 (by day 10), mice were i.p. injected with either LDL-PBS (100µM cholesterol, n=4), cisplatin (20 mg/kg, n=5), or LDL-Cis (100µM cholesterol, 20mg/kg cisplatin, n=5). Mice were euthanized 4

days later and weight loss **(B)** and tumor volume **(C)** were determined. Data are represented as mean value +/- SEM. **: $p<0.01$, ***: $p<0.001$, arrow indicates first injection. **D:** To evaluate cisplatin nephrotoxicity, kidney samples were recovered for IHC hematoxylin eosin staining. Images, taken in random fields, are representative of five pictures taken for each condition. n=4-5 mice per group. **E:** quantification of the percentage of lesion area reported to total field area (black arrow) is represented as mean value +/- SEM. **: $p<0.01$. **F**: Apoptosis in organs was assessed by IHF in kidney and liver. Histological slides were labeled with a cleaved caspase-3 antibody (Green) and with DAPI. Images are representative of five pictures taken for each condition. n=4, scale bar = 20µm. **G, H:** Quantifications of the immune-fluorescence intensity of Cleaved Caspase-3 in kidneys **(G)** or tumor **(H)** sections. Data are represented as mean increase vs. PBS +/- SEM. n=4-5 mice per group, **: $p<0.01$, ***: $p<0.001$. *P* values were calculated using one-way ANOVA.

Fig. 7.

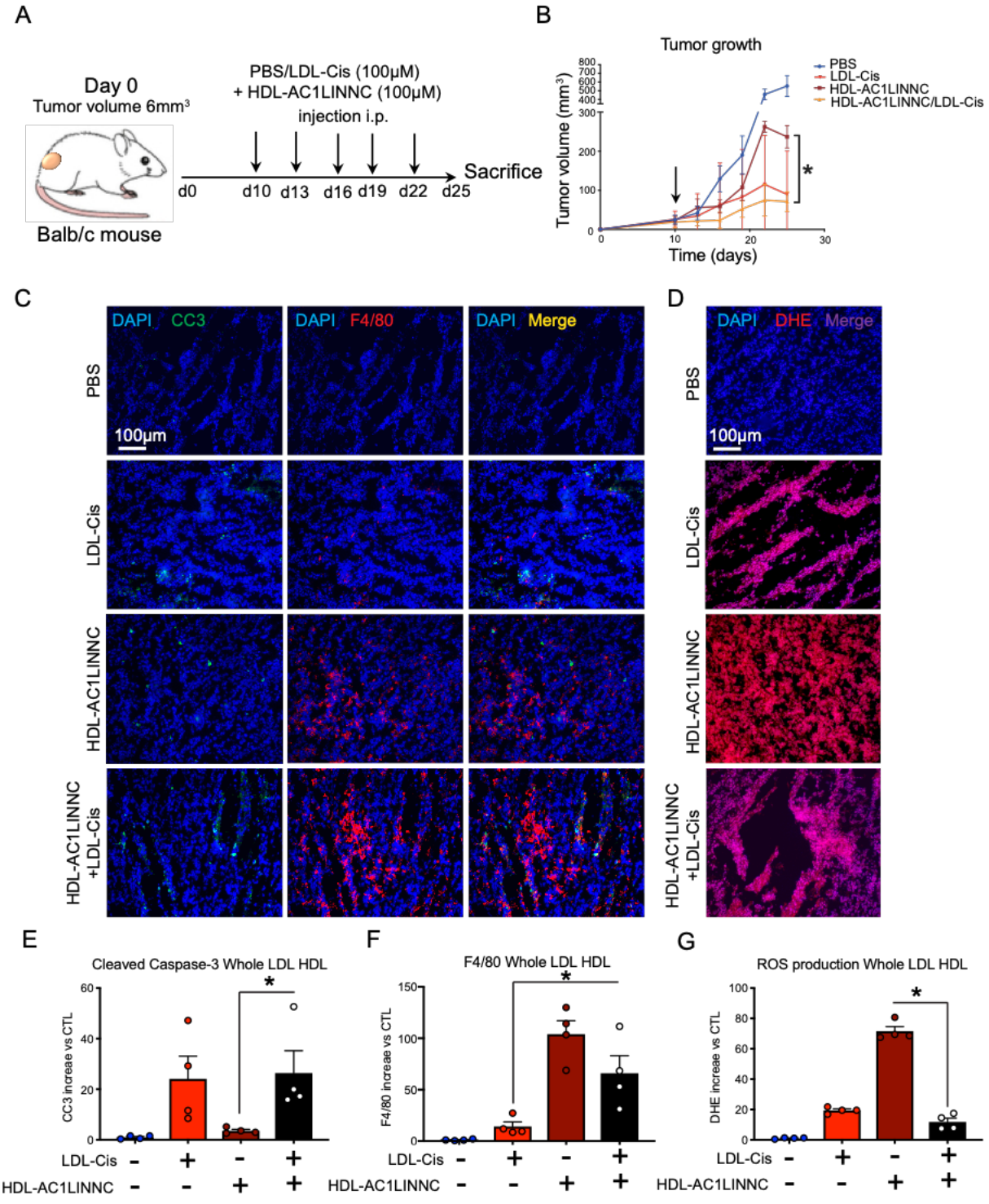

Figure 7: In vivo additive effect of cisplatin loaded LDL and AC1LINNC loaded HDL. A: Balb-c mice were injected with CT-26 colorectal cancer cells (10^6 cells/mice, *s.c.*). At the indicated times mice were treated either with PBS, HDL-AC1LINNC (100µM cholesterol, 10µM AC1LINNC, 100µl/mouse) or LDL-Cisplatin (100µM cholesterol, 1.5mg/kg cisplatin) + HDL-AC1LINNC (100µM cholesterol,

10µM AC1LINNC, 100µl/mouse). n=5 mice per group. **B:** Tumor volume was measured every 3 days and represented as mean value +/- SEM. *: $p<0.05$, arrow indicates first injection. **C:** Apoptosis and macrophage infiltration were determined in histological slides labeled with a cleaved caspase-3 antibody (Green) and a F4/80 antibody (Red), and with DAPI. Images were chosen in random fields and are representative of five pictures taken for each condition. n=5, scale bar = 50µm. **D:** ROS production in tumors was measured in histological slides by DAPI/DHE staining. Pictures, taken in random fields, are representative of five pictures taken for each condition. n=5, scale bar = 50µm. **E, F & G:** Quantifications of the immune-fluorescence intensity of Cleaved Caspase-3 **(E)**, F4/80 **(F)** and DHE **(G)**. Data are represented as mean increase vs. non treated +/- SEM. n=4, *: $p<0.05$, ****: $p<0.0001$. *P* values were calculated using one-way ANOVA.

References

1. Mantovani A, Marchesi F, Malesci A, Laghi L, and Allavena P. Tumour-associated macrophages as treatment targets in oncology. *Nat Rev Clin Oncol.* 2017;14(7):399-416.
2. Shapouri-Moghaddam A, Mohammadian S, Vazini H, Taghadosi M, Esmaeili SA, Mardani F, et al. Macrophage plasticity, polarization, and function in health and disease. *J Cell Physiol.* 2018;233(9):6425-40.
3. Pathria P, Louis TL, and Varner JA. Targeting Tumor-Associated Macrophages in Cancer. *Trends Immunol.* 2019;40(4):310-27.
4. Gobbo J, Marcion G, Cordonnier M, Dias AMM, Pernet N, Hammann A, et al. Restoring Anticancer Immune Response by Targeting Tumor-Derived Exosomes With a HSP70 Peptide Aptamer. *J Natl Cancer Inst.* 2016;108(3).
5. Madias NE, and Harrington JT. Platinum nephrotoxicity. *Am J Med.* 1978;65(2):307-14.
6. Gietema JA, Sleijfer DT, Willemse PH, Schraffordt Koops H, van Ittersum E, Verschuren WM, et al. Long-term follow-up of cardiovascular risk factors in patients given chemotherapy for disseminated nonseminomatous testicular cancer. *Ann Intern Med.* 1992;116(9):709-15.
7. Oberoi HS, Nukolova NV, Kabanov AV, and Bronich TK. Nanocarriers for delivery of platinum anticancer drugs. *Adv Drug Deliv Rev.* 2013;65(13-14):1667-85.
8. Kotelevets L, Chastre E, Caron J, Mougin J, Bastian G, Pineau A, et al. A Squalene-Based Nanomedicine for Oral Treatment of Colon Cancer. *Cancer Res.* 2017;77(11):2964-75.
9. Jego G, Lanneau D, De Thonel A, Berthenet K, Hazoume A, Droin N, et al. Dual regulation of SPI1/PU.1 transcription factor by heat shock factor 1 (HSF1) during macrophage differentiation of monocytes. *Leukemia.* 2014;28(8):1676-86.
10. Wang R, Kovalchin JT, Muhlenkamp P, and Chandawarkar RY. Exogenous heat shock protein 70 binds macrophage lipid raft microdomain and stimulates phagocytosis, processing, and MHC-II presentation of antigens. *Blood.* 2006;107(4):1636-42.
11. Rerole AL, Gobbo J, De Thonel A, Schmitt E, Pais de Barros JP, Hammann A, et al. Peptides and aptamers targeting HSP70: a novel approach for anticancer chemotherapy. *Cancer Res.* 2011;71(2):484-95.
12. Barenholz Y. Doxil(R)--the first FDA-approved nano-drug: lessons learned. *J Control Release.* 2012;160(2):117-34.
13. Allen TM, and Cullis PR. Liposomal drug delivery systems: from concept to clinical applications. *Adv Drug Deliv Rev.* 2013;65(1):36-48.
14. Seetharamu N, Kim E, Hochster H, Martin F, and Muggia F. Phase II study of liposomal cisplatin (SPI-77) in platinum-sensitive recurrences of ovarian cancer. *Anticancer Res.* 2010;30(2):541-5.
15. Veal GJ, Griffin MJ, Price E, Parry A, Dick GS, Little MA, et al. A phase I study in paediatric patients to evaluate the safety and pharmacokinetics of SPI-77, a liposome encapsulated formulation of cisplatin. *Br J Cancer.* 2001;84(8):1029-35.
16. Stathopoulos GP, and Boulikas T. Lipoplatin formulation review article. *J Drug Deliv.* 2012;2012:581363.
17. de Jonge MJ, Slingerland M, Loos WJ, Wiemer EA, Burger H, Mathijssen RH, et al. Early cessation of the clinical development of LiPlaCis, a liposomal cisplatin formulation. *Eur J Cancer.* 2010;46(16):3016-21.
18. Boulikas T, and Vougiouka M. Cisplatin and platinum drugs at the molecular level. (Review). *Oncol Rep.* 2003;10(6):1663-82.
19. Newman MS, Colbern GT, Working PK, Engbers C, and Amantea MA. Comparative pharmacokinetics, tissue distribution, and therapeutic effectiveness of cisplatin encapsulated in long-circulating, pegylated liposomes (SPI-077) in tumor-bearing mice. *Cancer Chemother Pharmacol.* 1999;43(1):1-7.
20. Firestone RA. Low-density lipoprotein as a vehicle for targeting antitumor compounds to cancer cells. *Bioconjug Chem.* 1994;5(2):105-13.

21. Goldstein JL, and Brown MS. The LDL receptor. *Arterioscler Thromb Vasc Biol.* 2009;29(4):431-8.
22. Hadi T, Douhard R, Dias AMM, Wendremaire M, Pezze M, Bardou M, et al. Beta3 adrenergic receptor stimulation in human macrophages inhibits NADPHoxidase activity and induces catalase expression via PPARgamma activation. *Biochim Biophys Acta Mol Cell Res.* 2017;1864(10):1769-84.
23. Redgrave TG, Roberts DC, and West CE. Separation of plasma lipoproteins by density-gradient ultracentrifugation. *Anal Biochem.* 1975;65(1-2):42-9.
24. Duheron V, Moreau M, Collin B, Sali W, Bernhard C, Goze C, et al. Dual labeling of lipopolysaccharides for SPECT-CT imaging and fluorescence microscopy. *ACS Chem Biol.* 2014;9(3):656-62.
25. Bernhard C, Goze C, Rousselin Y, and Denat F. First bodipy-DOTA derivatives as probes for bimodal imaging. *Chem Commun (Camb).* 2010;46(43):8267-9.